Hindawi
International Journal of Corrosion
Volume 2018, Article ID 9078253, 18 pages
https://doi.org/10.1155/2018/9078253

Research Article

Inhibition Effect of Natural Pozzolan and Zinc Phosphate Baths on Reinforcing Steel Corrosion

Aref M. al-Swaidani

Associate Professor, Faculty of Architectural Engineering, Arab International (Formerly European) University, Damascus, Syria

Correspondence should be addressed to Aref M. al-Swaidani; aydlswaidani@yahoo.fr

Received 26 January 2018; Accepted 24 May 2018; Published 2 July 2018

Academic Editor: Tuan A. Nguyen

Zinc phosphate (ZnP) baths are widely used for increasing corrosion resistance and surface preparation for painting. Studies on exploiting these baths in the reinforced concrete (RC) are still in the early stages. This is probably due to the shortcomings, such as the alkaline instability and high porosity of the obtained coatings. Use of natural pozzolan (NP) as cement replacement is growing rapidly due to its economic, ecological, and technical benefits. The combined effect of using ZnP baths and NP-based cement on the resistance of concrete against damage caused by corrosion has been investigated. Four phosphating baths were prepared: ZnP, ZnP-Ni, ZnP-Cu, and ZnP-Mn. Steel specimens were phosphated at 55-60°C for 15 min. Concrete specimens were produced with four different levels of NP: 0% (control), 10 %, 20%, and 30%. The investigation was carried out using RC specimens where a constant anodic potential was impressed after 28 and 90 days of concrete curing. The electrochemical behavior of the coated steel has further been evaluated in chloride contaminated $Ca(OH)_2$ saturated solution (CH-Cl) using the open circuit potential (OCP), the potentiodynamic polarization, and the polarization resistance with time. The bond strength between the coated steel and concrete has been evaluated by the pull-out test. Test results showed that concrete containing NP at higher replacement levels and steel specimens treated in bication baths exhibited corrosion initiation times several times longer than the control concrete with uncoated steel. In addition, the best corrosion performance was noted in the steel specimen treated in the ZnP-Cu bath. Its corrosion density was about twentyfold lower with respect to the bare steel, and its inhibition efficiency exceeded 95% in (CH-Cl) solution. In addition, its polarization resistance was about fifteenfold lower with respect to the bare steel. SEM, EDX, and XRD techniques have been employed, as well.

1. Introduction

Reinforcing steel embedded in fresh concrete develops a protective passive layer on its surface. This layer, which is formed as a result of the high alkalinity of the concrete pore solution (pH ~ 13), consists of γ-Fe_2O_3 adhering tightly to the steel. As long as that oxide film is present, the steel remains intact [1]. However, chloride ions attack and concrete carbonation can destroy the film and, in the presence of H_2O and O_2, reinforcement corrosion takes place. Chloride ions, which were described by Verbeck [2] as the specific and unique destroyer, can be present in concrete through the use of either contaminated aggregate, sea water, brackish water, or admixtures containing chlorides [1].

In the literature, there are state-of-the-art review studies on numerous methods of protection against reinforcement corrosion [3–8]. A variety of protective coatings such as zinc and epoxy coatings have widely been used to improve the corrosion resistance of reinforcing bars. Treatments of reinforcing steel in zinc phosphate baths could probably be a vital approach in the future [9–12].

The phosphating process has been known for over a century [13]. It was extensively used in the automobile and appliance industries [14, 15]. This treatment primarily provides an inexpensive [15, 16], nontoxic [17, 18], reasonably hard, highly adherent, and electronically nonconducting phosphate coating [13].

The insulation properties make an important contribution to the prevention of reinforcement corrosion [19]. Further, the zinc phosphate baths are currently considered eco-friendly [20]. However, the obtained phosphate coatings usually contain pores which are pathways for the corrosive

electrolyte diffusion into the metal substrate. As a result, the corrosion resistance of the conventional phosphate coating is not high enough. Additives such as Ni^{2+}, Cu^{2+}, Mn^{2+}, Ca^{2+}, and Mo^{2+} and nanoparticles have been extensively used to produce phosphate coatings with uniform structure, lower porosity, higher corrosion resistance, and improved adhesion properties [11, 15, 21–25]. A brief state-of-the-art review of these additives and their effects on the characteristics of zinc phosphate baths has recently been published by the author [26].

Zinc phosphating is essentially an electrochemical process [27]. When the steel comes into contact with phosphate solution which is basically a phosphoric acid-based solution, an electrochemical reaction takes place. Fe^{2+} ions start to dissolve and release electrons at the anodic site, and the reduction of H^+ occurs at the cathodic site. The evolution of hydrogen and consumption of H^+ ions result in a local increase of pH at the surface leading to precipitation of zinc phosphate crystals [28]. According to Zimmermann et al. [23], Donofrio [29], and Kunst et al. [30], the possible reactions taking place in the zinc phosphating bath are as follows:

$$3Zn^{2+} + 2H_2PO_4^- + 4H_2O \longrightarrow Zn_3(PO_4)_2.4H_2O\ (\text{Hopeite}) + 4H^+ \quad (1)$$

$$2Zn^{2+} + Fe^{2+} + 2H_2PO_4^- + 4H_2O \longrightarrow Zn_2Fe(PO_4)_2.4H_2O\ (\text{Phosphophyllite}) + 4H^+ \quad (2)$$

The alkaline stability of the obtained zinc phosphate coating on steel is of great importance, as it will be embedded in a highly alkaline environment (pH~13). Literature shows that the alkaline stability of zinc phosphate coatings depends on their chemical composition and crystal structure [31]. Hopeite ($Zn_3(PO_4)_2.4H_2O$) has a higher alkaline solubility than phosphophyllite ($Zn_2Fe(PO_4)_2.H_2O$) [29, 32, 33]. Thus, alkaline solutions first dissolve the coating composed of hopeite. Then the dissolution continues for layers rich in iron and those mainly composed of phosphophyllite [34]. In general, the presence of phosphophyllite is associated with a better corrosion resistance than hopeite, probably due to its enhanced chemical stability relative to alkaline electrolytes [35].

Natural pozzolan (NP) is being widely used as cement replacement due to its ecological, economic., and performance-related advantageous properties [36–41]. However, its use caused a lower alkalinity compared with plain Portland cement [42]. This could be due to the reduction in cement content (i.e., the dilution effect) when adding natural pozzolan and the consumption of portlandite (CH) through the pozzolanic reaction.

Syria is rich in natural pozzolan with estimated reserves of about one billion tonnes [43]. There are a significant number of studies that deal separately with the effect of using natural pozzolan or that of zinc phosphating process on the corrosion of reinforcing steel. However, very little or even no previous works, as the author thinks, have been carried out in the past to investigate the combined effect of adding NP as cement replacement and zinc phosphate coated steel on the anticorrosion properties of reinforcing steel exposed to highly chloride ion concentrations. In addition, literature did not cover the benefit, in terms of alkaline stability, which can be achieved when the zinc phosphate coated steel is embedded in concrete of relatively lower alkalinity. Further, the reduced concrete permeability offered by NP-based cements could be considered an additional physical barrier between steel and its environment.

The objective of this paper is to investigate the influence of adding NP as cement replacement on the corrosion performance of reinforcing steel treated in different zinc phosphate baths. Four binders with different replacement levels of NP (0%, 10%, 20%, and 30%) have been produced for this investigation. In addition, four zinc phosphating baths were employed: the first one is a monocation bath (i.e., it contains only Zn-cation) and three bication baths, Zn-Ni, Zn-Cu, and Zn-Mn, respectively. Two test environments were created for this investigation: concrete specimens and a contaminated $Ca(OH)_2$ saturated solution in which the coated steel was embedded or immersed.

The study is of particular importance for the following points:

(i) Replacement of OPC by natural pozzolan could significantly minimize CO_2 released into atmosphere and save energy. In addition, zinc phosphating process is considered eco-friendly.

(ii) This study is the first of its kind in Syria. However, it is not limited to the country. It can be applied to other countries of similar geology, e.g., Harrat Al-Shamah, a volcanic field which covers a total area of some 45,000 km^2, and about 15,000 km^2 is located in the country. The rest covers parts of Jordan and KSA.

(iii) As our country begins preparations for the huge reconstruction after the war comes to its end, the encouraging results can be considered a motivation of other studies, for instance, use of these local supplementary cementing materials in enhancement of the anticorrosion properties of reinforced concrete made from recycled concrete aggregates (RCA). RCA are expected to be an inevitable building material during the postwar reconstruction in Syria.

2. Experimental Procedure

2.1. NP-Based Concrete. Natural pozzolan (NP) used in the experiments was collected from a Tal Shihan quarry, 70 km southeast of Damascus. More detailed information related to its characteristics can be found in the latest research work of the author and colleagues [44].

Four binder specimens have been prepared: one plain Portland cement CEM I (control) and three binary binders with three replacement levels of 10%, 20%, and 30% NP (EN 197-1). 5% of gypsum was added to all the binder specimens. This ratio is frequently used by all Syrian cement plants, providing about 2.35% SO_3 content. The amount of gypsum added to the cement clinker is expressed usually as the

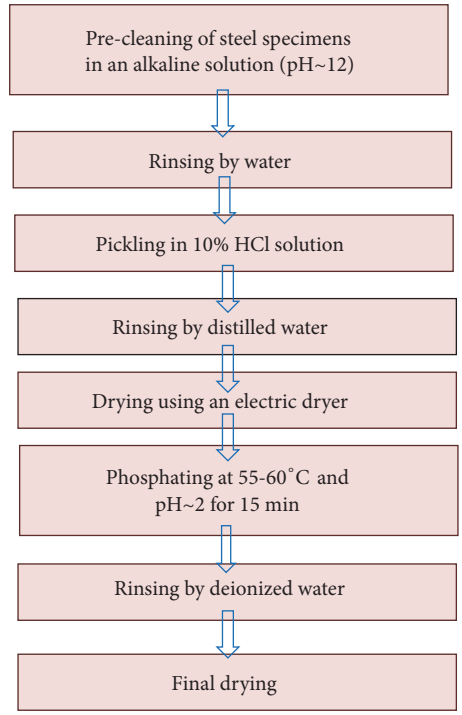

Figure 1: A schematic representation of the full steps of phosphating process.

mass of SO_3 present; this is limited by European Standard BS EN 197-1: 2000 to a maximum of 3.5 percent [45]. All replacements were made by mass of cement. All binders were designated according to the replacement level. For instance, NP10 and NP30 refer to the binders containing 10% and 30% of NP, respectively. More data on the characteristics of the binder components, namely, particle size distribution and the grinding method, can also be found in the scientific work of the author and colleagues [44].

Four concrete mixes have been prepared using the same constituents and procedure followed by the author in his latest work [44]. Concrete cubes (150 mm) were cast for the determination of compressive strength and water permeability. Concrete cylinders of 75 mm × 150 mm and 100 mm × 200 mm were also cast for testing the concrete porosity and the concrete chloride ion penetrability, respectively. The RC specimen for the accelerated corrosion test was 100 mm × 200 mm concrete cylinder in which 14 mm diameter steel bar was centrally embedded. The steel bar was embedded into the concrete cylinder such that its end was at least 45 mm from the bottom of the cylinder, and it was coated with epoxy at the exit from the concrete cylinder in order to eliminate crevice corrosion.

2.2. Zinc Phosphate Baths. Four zinc phosphate baths were created, conventional bath or monocation bath without modifying elements and three bication baths modified either by nickel (Ni^{2+}), copper (Cu^{2+}), or manganese (Mn^{2+}) cations. Their chemical compositions and designations are illustrated in Table 1. All the chemical reagents applied in the present work were of analytic grade. Deionized water was used in all zinc phosphating baths. Phosphating process was carried out by the conventional immersion of reinforcing steel specimens at 55-60°C, for 15 min in the phosphating baths at a pH value of 2±0.1. The phosphating process primarily included precleaning, activation, phosphating, rinsing, and drying. The full steps of the phosphating process are schematically illustrated in Figure 1. The chemical composition of steel rebar with some mechanical properties is presented in Table 2. A macrograph of treated steel specimens with an optical microscopic photo is shown in Figure 2. A ZnP-Ni coating of about 8 μm thickness can clearly be seen in Figure 2(b).

2.3. Morphology of Zinc Phosphate Coatings. The morphology and elemental composition of the obtained zinc phosphate coatings were studied by scanning electron microscope (SEM, VEGA II TESCAN) and energy disperse X-ray (EDX) spectrometer.

2.4. Mechanical and Durability-Related Tests of Concrete

2.4.1. Compressive Strength, Water Permeability, Chloride Ion Penetrability, and Porosity Tests. The compressive strength development of concrete was conducted on 150 mm cubic concrete specimens in accordance with ISO 4012, at ages of 28 and 90 days. Concrete permeability measured in terms of depth of water penetration has been carried out as per the standard EN 12390-8. The results shown in this paper are the average penetration depth. The rapid chloride penetrability (RCP) test was conducted in accordance with ASTM C1202. Three cylinder specimens of each concrete mix were tested after 28 and 90 days of curing. Porosity measurements were conducted using vacuum saturation method in accordance with RILEM CPC 11.3. The results

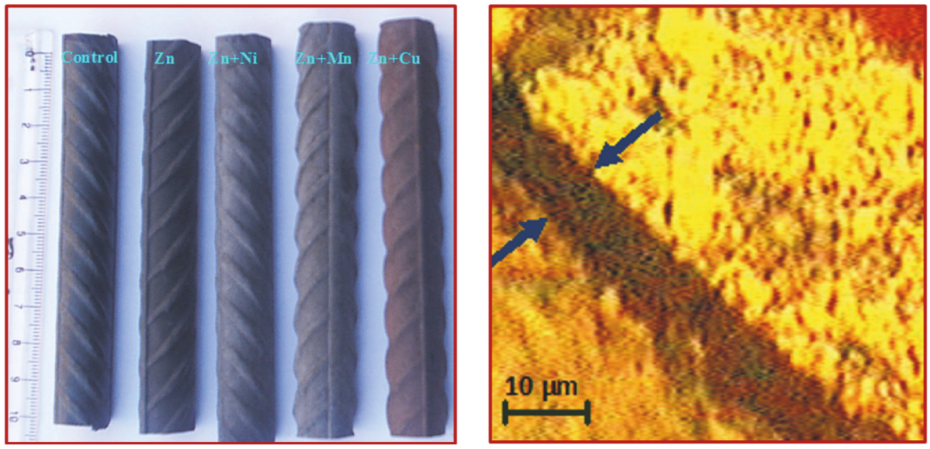

(a) (b)

Figure 2: (a) Photograph of the some phosphated steel rebars; (b) an optical microscopy photo of cross-sectional ZnP-Ni treated steel.

Table 1: Chemical composition of the prepared zinc phosphating baths.

Bath type	Designation	Concentration (Mole/l)					
		PO_4^{3-}	NO_3^{1-}	Zn^{2+}	Ni^{2+}	Cu^{2+}	Mn^{2+}
Mono-cation bath (conventional)	ZnP	0.34	0.14	0.17	0	0	0
Bi-cation baths	ZnP-Ni	0.34	0.14	0.17	0.017		
	ZnP-Cu	0.34	0.14	0.17		0.017	
	ZnP-Mn	0.34	0.14	0.17			0.017

Table 2: Chemical composition with some physical characteristics of the steel bars used in the experiments.

Rebar type	Chemical composition (%)							Mechanical properties		
	C	Si	Mn	P	S	Ni	Cu	Elastic point (MPa)	Tensile strength (MPa)	Elongation (%)
14 mm (RB 400)	0.23	0.11	0.54	0.006	0.009	0.001	0.001	488.7	638.2	15

reported represent the average of six readings for compressive strength test and the average of three readings for all other tests.

2.4.2. Accelerated Corrosion Test. A rapid corrosion test was used to compare the corrosion performance of NP-based cement concrete in which either straight phosphate rebars or bent phosphate rebars are embedded, as shown in Figure 3. The objective of evaluating the bent phosphated rebars is to verify the coating soundness and to investigate whether or not the bending action might affect its corrosion performance. Similar techniques with little differences were reported by other researchers [36, 46–50]. The cylindrical specimen shape was adopted to provide uniform cover and easier fabrication. In the study, RC specimens were immersed in a 15 % NaCl solution leveling half of the concrete cylinder and the steel bar (working electrode) was connected to the positive terminal of a DC power source while the negative terminal was connected to a steel plate (counter electrode) placed near the concrete specimen in the solution. The corrosion process was initiated by impressing a relatively high anodic potential of 12 V to accelerate the corrosion process. The instrument used in the test is a Laboratory DC power supply, Model GPC-60-300 equipped with a Digital Multimeter Sanwa, CD 721.

Figure 3 shows a schematic representation of the experimental setup for the accelerated corrosion test. The specimens were monitored periodically to see how long it takes for corrosion cracks to appear on the specimen surface. The current readings with time were recorded at 3 h intervals. Three specimens from each concrete mix and phosphating bath were tested after 28 and 90 days of curing.

2.4.3. Bond Strength Test. Pull-out tests and beam tests are the common experimental methods used for assessment of bond performance [51]. In the study, the concrete cube specimens were tested to determine the bond strength between steel rebars and concrete using the concentric pull-out test. This concentric pull-out test was similar to that outlined in ASTM C 234. Although this type of test does not represent the actual situation in a structure, the authors used this method since the study is basically a comparative study. The pull-out test was carried out using 150 mm cubic specimens with the bar centrally embedded. Deformed steel bars with 16 mm in diameter were used instead of no. 6 (19 mm) bars specified in ASTM C 234 which is used as the basis of casting and testing procedures. Each mold was designed to cast one 150 mm cubic specimen as shown in Figure 4(a). The mold was made of steel plates. The

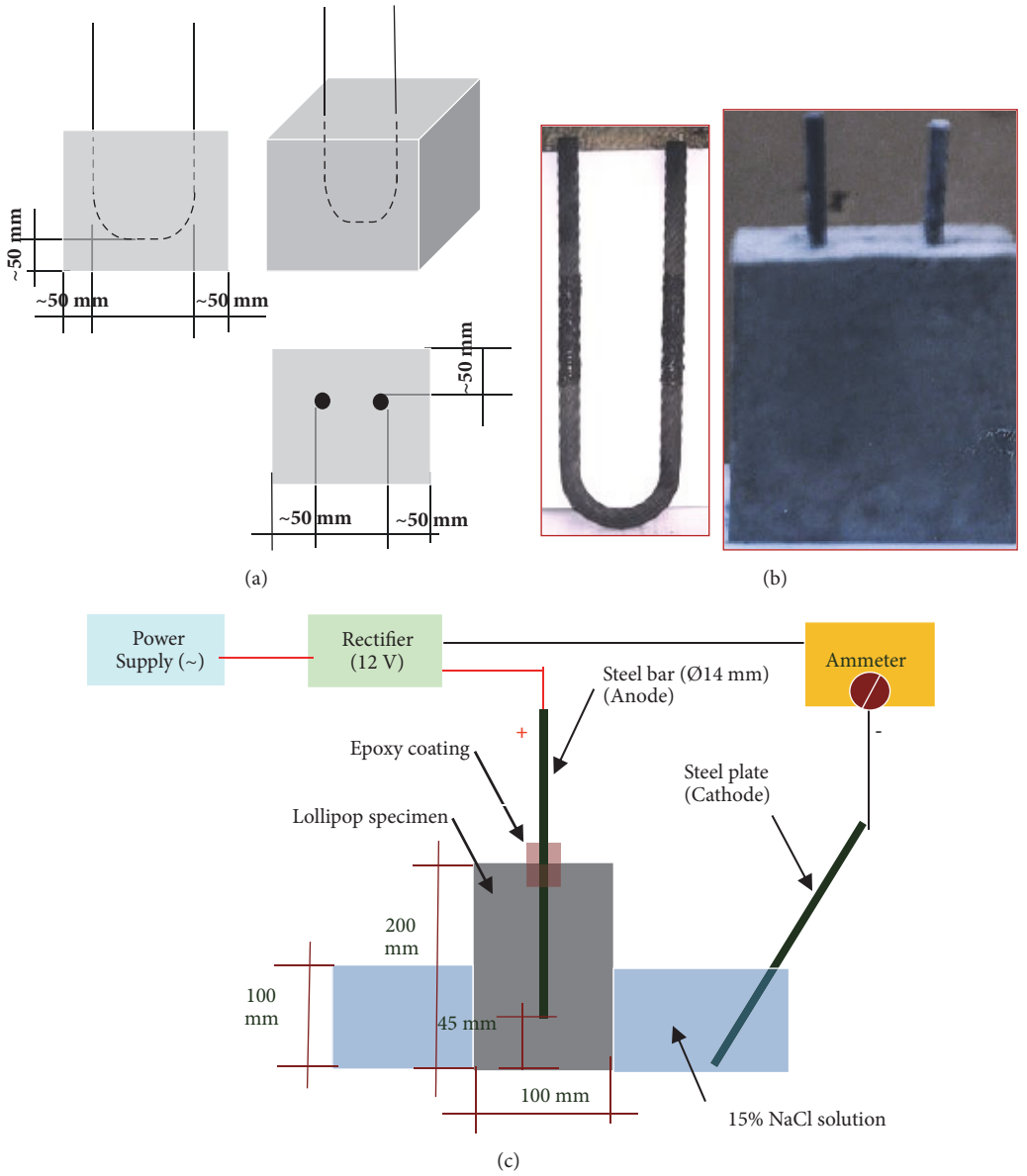

FIGURE 3: ((a) and (b)) Schematic representation of the concrete specimen with bent steel rebar. (c) Schematic representation of experimental setup for the accelerated corrosion test.

holed cap was designed to support the bar in a vertical position.

The embedment length of reinforcing bars was 72 mm (~4.5 times the rebar diameter). The required embedment length has been obtained by breaking the bond between steel and concrete using polyvinyl chloride (PVC) sleeves to cover the unembedded length. The gap between the reinforcing steel and sleeves was sealed with a silicon sealant.

Sketch map of the bond test setup and a photograph of the bond test frame with the specimen in position are shown in Figures 4(b) and 4(c). The specimen was mounted in the frame with the bar passing through the slot in the frame. A digital dial indicator has been installed on the free end to measure the rebar's displacements.

A 2000 kN capacity universal testing machine has been used for the pull-out testing. The bond stress (τ) has been calculated by dividing the applied load (F) by the surface area ($\pi \text{Ø} l$) of reinforcing steel in contact with concrete, as shown in the following formula:

$$\tau = \frac{F}{\pi \text{Ø} l} \tag{3}$$

where l is the length of embedment (72 mm) and Ø is the diameter of the reinforcing bar (16 mm).

The free-end slip values were plotted against the bond stresses, and the bond strengths at failure have been determined for each concrete mixture and curing age.

2.5. Tests in Chloride Contaminated $Ca(OH)_2$ Saturated Solution. A saturated $Ca(OH)_2$ solution with an approximate pH of 12.5 was used to simulate the pore solution existing in concrete. 3.5% NaCl was added to the saturated $Ca(OH)_2$

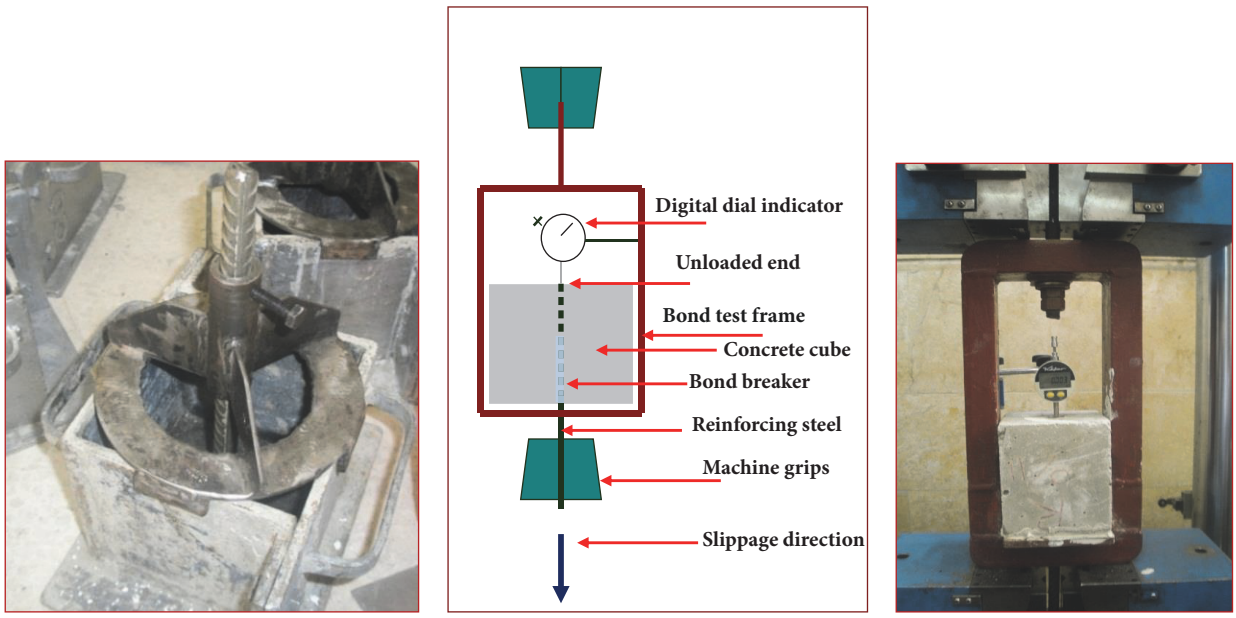

(a) (b) (c)

FIGURE 4: **(a)** Photograph of the mold used in the bond test with the bar in place; (b) sketch map of the bond set up; **(c)** photograph of the bond test setup with the specimen in position.

solution to simulate reinforced concrete exposed to chloride attack. The obtained chloride contaminated solution is denoted (CH-Cl). Its pH value was about 12.3. In numerous studies of reinforcement corrosion, saturated $Ca(OH)_2$ has been used as a substitute for concrete pore solution [52].

The electrochemical tests in the (CH-Cl) solution were performed with a three-electrode system. The working electrode was either the coated steel or the bare steel, the counter electrode was a platinum sheet, and the reference electrode was a saturated Calomel electrode (SCE). The surface area of the working electrode exposed to the solution was 6 cm^2. Different electrochemical methods were employed to evaluate the corrosion behavior of the coated steel specimens. First, the coated and bare steel specimens were immersed in the test solution for one hour to reach stationary open circuit potential (OCP). Second, polarization curves have been measured with a scan rate of 0.5 mV/s and a scan range from -0.25 V for OCP to + 0.25 V for pitting potential. Third, periodic measurements of linear polarization resistance (LPR) over time were performed during 96 h. The specimens were polarized at ±20 mV with respect to the open circuit potential (E_{ocp}) at a scan rate of 0.5 mV/s and the LRP measurements were taken every 30 minutes. For a small perturbation about the open circuit potential, there is a linear relationship between the change in applied current per unit area of electrode (Δi) and the change of the measured voltage (ΔE). The ratio ($\Delta E/\Delta i$) is called polarization resistance (R_p). The testing temperature was 25°C.

After the test, the specimens were rinsed at room temperature and the surface was observed and analysed with SEM and EDX. SATOE STADI X-ray diffractometer (XRD) using CuKα radiation, operated at 40 KV and 30 mA with a scan mode ranging from 5 to 85° and a scan speed of 2°/min, was also employed in order to investigate the phases formed on the coated steel surface after immersion in (CH-Cl) solution.

All the electrochemical tests were performed using a potentiostat (TACUSSEL, PGZ 301) at ambient temperature. The tests were repeated three times with the same conditions for confirming the reproducibility of the obtained zinc phosphate coatings. All electrochemical experiments were remarkably reproducible.

3. Results and Discussion

3.1. Morphology and Chemical Composition of Zinc Phosphate Coating. Scanning electron micrographs of the zinc phosphate coatings obtained during the phosphating process are shown in Figures 5–8. The SEM observations give more detail about the modifications of coating morphology with the cation type in the phosphating solutions.

For the monocation bath, ZnP bath, the coating seems to be porous. It consists of platelet shaped crystallites of 30–40 μm length and 5–10 μm width, which uniformly covered the surface of the specimen, Figure 5. However, the presence of Ni^{2+}, Cu^{2+}, and Mn^{2+} cations in the phosphating solutions resulted in a significant modification of the crystalline form and size.

The ZnP-Ni coating is smoother than the monocation ZnP coating. Its structure is characterized by platelets with sizes up to 20 μm in length and up to 3 μm in width, as shown in Figure 6. The grain refinement was also reported in literature [9, 35, 53, 54]. The relatively high weight of Ni in the coating as confirmed by the EDX analysis may indicate the substitution of Zn^{2+} by Ni^{2+} in hopeite or the deposition of Ni in the coating. This result was in agreement with the results obtained by Zimmermann et al. [23] and Su and Lin

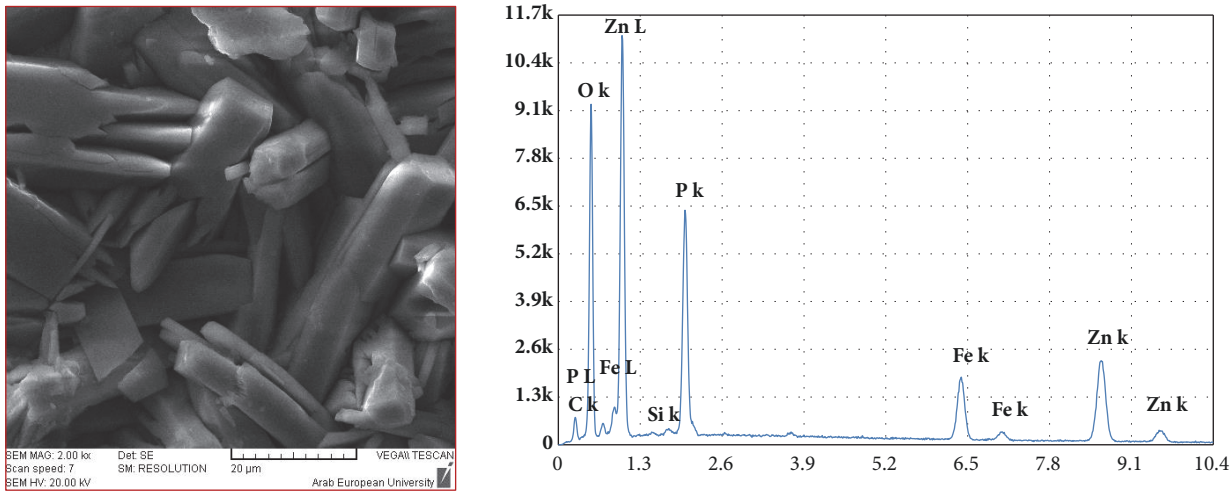

Figure 5: SEM and EDX of ZnP coating.

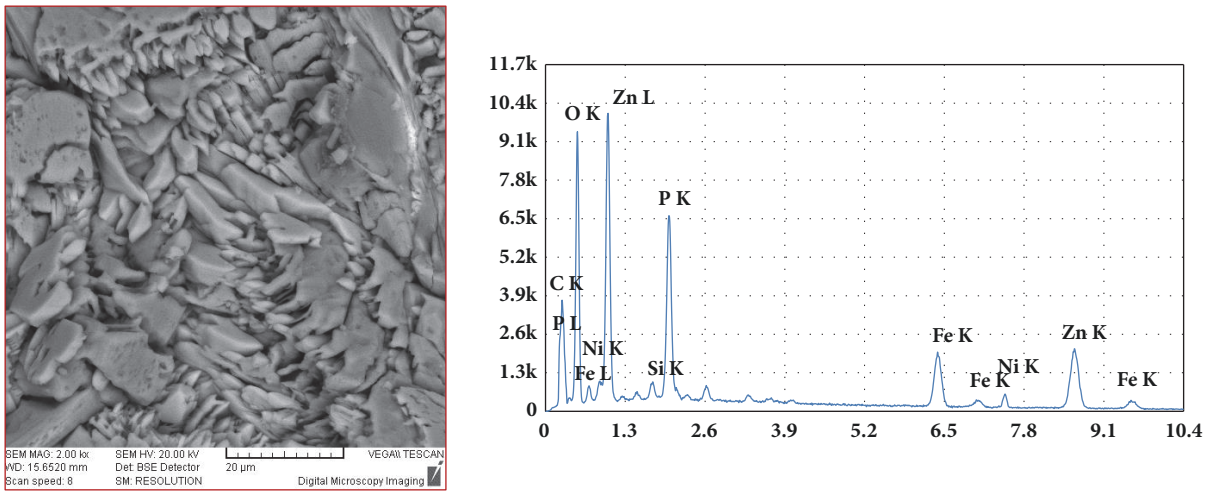

Figure 6: SEM and EDX of ZnP-Ni coating.

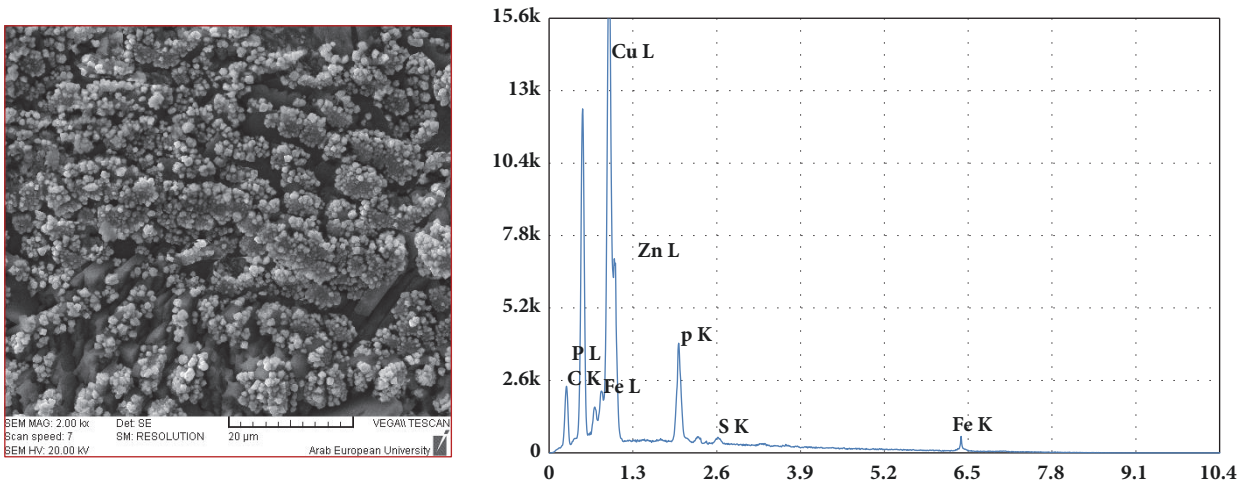

Figure 7: SEM and EDX of ZnP-Cu coating.

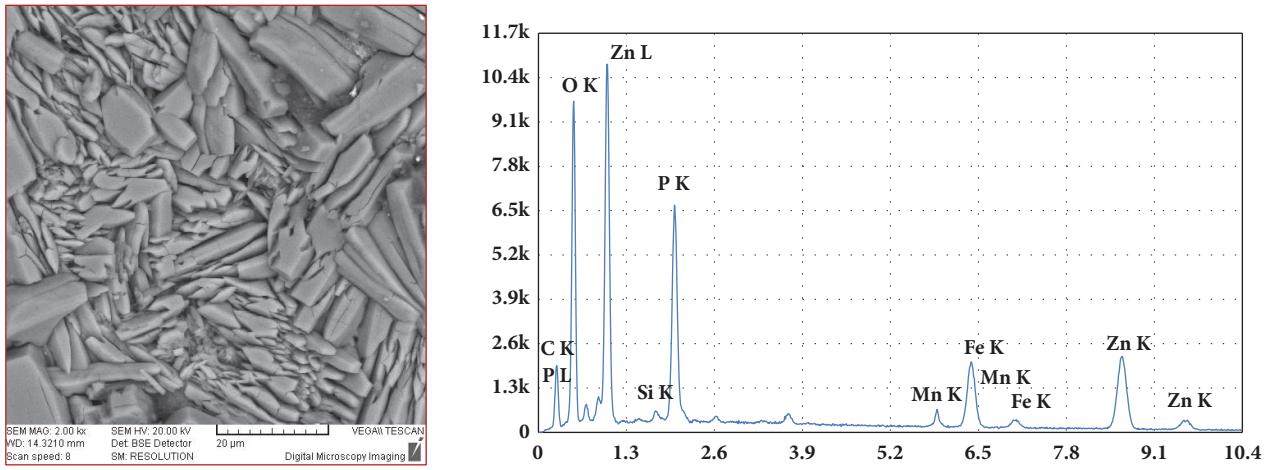

FIGURE 8: SEM and EDX of ZnP-Mn coating.

[55] who proposed the formation of $Zn_{(3-x)}Ni_x(PO_4)_2.yH_2O$. According to Kulinich and Akhtar [56], Ni^{2+} has two main roles in the zinc phosphate coating mechanism. First, the rate of increase in local solution pH is limited by the slower kinetics of reactions involving Ni^{2+} compared to Zn^{2+}, leading to thinner zinc phosphate coatings when Ni^{2+} is present in the coating solution. Second, most Ni^{2+} deposition occurs during the later stages of the coating process, by nickel phosphate deposition and formation of Ni-rich corrosion-resistant oxide.

The ZnP-Cu coating consists of smaller grains, the dimensions of which varied between 2 and 6 μm. Copper, as clearly seen in Figure 7, modified and refined the crystal structure and enhanced the coverage of the surface significantly. This, which was in agreement with the results obtained by Abdalla et al. [57], can be attributed to the effect of CU-Fe galvanic couple on dissolution of iron and acceleration of crystal deposition [57]. From the EDX analysis, Figure 7, it can clearly be distinguished that the dominant element was copper. Therefore, the metal surface exposed between the formed crystals might be a surface of copper rather than the base metal. This result is in well agreement with the result of Ogle and Buchheit [35] who concluded that Cu^{2+} may deposit as copper metal on the surface.

From Figure 8, it is noted that the ZnP-Mn coating is well crystallized and it completely covers the steel surface. Its structure is characterized by small platelets whose width is about 3 μm and length is 15 μm. Manganese (Mn^{2+}) behavior, to some extent, in the phosphating bath is similar to that of Ni^{2+}, as clearly seen in Figure 8. In addition, Mn^{2+} may replace Zn^{2+} in the hopeite crystal lattice. The presence of Mn^{2+} in the coating may support this assumption, as clearly seen from the EDX analysis in Figure 8. This was in agreement with the results obtained by Su and Lin [55], who proposed the formation of $Mn_2Zn(PO_4)_2.4H_2O$. Rezaee et al. [21] also observed this formation. In addition, adding Mn^{2+} reduced the phosphate coating porosity and improved surface coverage which led to an enhanced corrosion resistance [21].

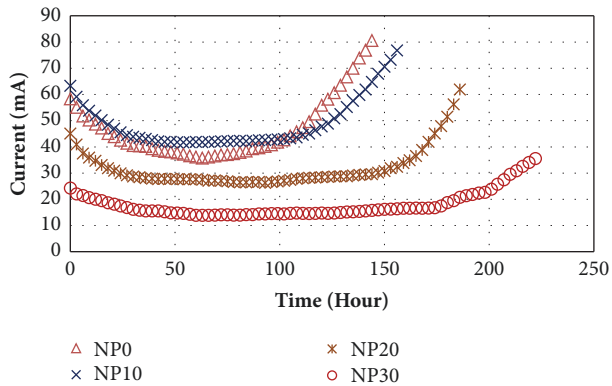

FIGURE 9: Typical curves of corrosion current versus time of concrete specimens tested after 28 days of curing.

3.2. Compressive Strength and Permeability-Related Properties of Concrete. Tables 3 and 4 show the test results of compressive strength, water penetration depth, chloride ion penetrability, and porosity of concrete. The test results will not be discussed here as the same trend of results using the same or a similar natural pozzolan was studied in depth in recent works carried out by the author [44, 58]. In addition, the microstructural investigation of the hydration products can also be found in these works.

3.3. Corrosion Resistance of Coated Steel Specimens Embedded in NP-Based Concrete. Typical curves of corrosion current versus time for the reinforced concrete specimens made with NP-based binders and phosphate steel rebars are illustrated in Figures 9–12, respectively. As shown in Figures 9–12, current-time curve initially descended till a time value after which a steady low rate of increase in current was observed, and after a specific time period a rapid increase in current was detected until failure. The decreasing tendency of current at the very early time could be explained by the filling of the pores with salt and other deposits in the salt water [36].

Table 3: Compressive strength development of concrete.

Mix type	Compressive (f_c) strength of concrete (MPa), normalized	
	28 days of curing	90 days of curing
NP0	42.1-100%	47.9-100%
NP10	40.1-95%	46.9-98%
NP20	34.2-81%	43.7-91%
NP30	32.3-77%	47.8-89%

Table 4: Water penetration depths, porosity, chloride penetrability, and pH of the investigated concrete.

Curing time	Binder type	Water penetration depth (mm)	Porosity (%)	Chloride penetrability (Coulombs)	pH
28 days	NP0	65	17.2	6278	12.65
	NP10	61	15.7	5891	12.34
	NP20	48	14.2	4367	12.08
	NP30	42	11.1	2915	12.01
90 days	NP0	53	14.4	3971	12.57
	NP10	43	12.2	3214	12.19
	NP20	29	9.7	1965	11.91
	NP30	22	6.8	1112	11.93

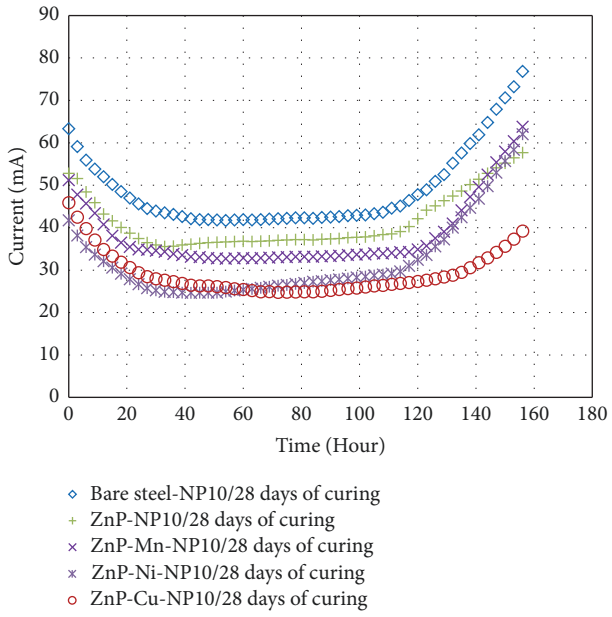

Figure 10: Time to cracking of RC specimens made with NP10-based cement and phosphated steel rebars after 28 days of curing.

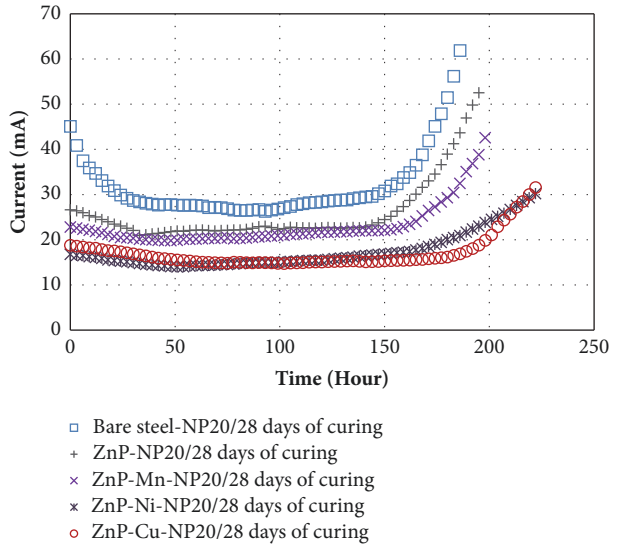

Figure 11: Time to cracking of RC specimens made with NP20-based cement and phosphated steel rebars after 28 days of curing.

Almost a similar variation of the corrosion current with time has also been observed by other researchers [46, 50]. The first visual evidence of corrosion was the appearance of brown stains on the surface of the specimens. Cracking was observed shortly thereafter, and it was associated with a sudden rise in the current.

Figure 13 presents the average corrosion times required to crack the specimens made with NP-based binders and phosphated steel rebars. Time to cracking in NP0-based concrete specimens was in the range of 87–134 h (3.6–5.6 days), whereas that in NP30-based concrete was in the range of 197–367 h (8.2–15.3 days). In addition, it was observed in Figure 13 that the corrosion resistance of NP-based cement concrete specimens increased significantly with age while that of the plain cement concrete had a slight increase which has also been indicated by other researchers [36, 50].

The combined effect of using NP-based cement concrete and zinc phosphated steel rebars can clearly be seen in Figure 13. From the graphs, it is very clear to note that the time taken for initiation of 28-day cured concrete cracking was found to be 197, 215, 246, 263, and 232 h for bare steel rebar, ZnP coated steel rebar, ZnP-Mn coated steel rebar, ZnP-Ni coated steel rebar, and ZnP-Cu coated steel rebar which were embedded in NP30-based concrete, respectively. The best

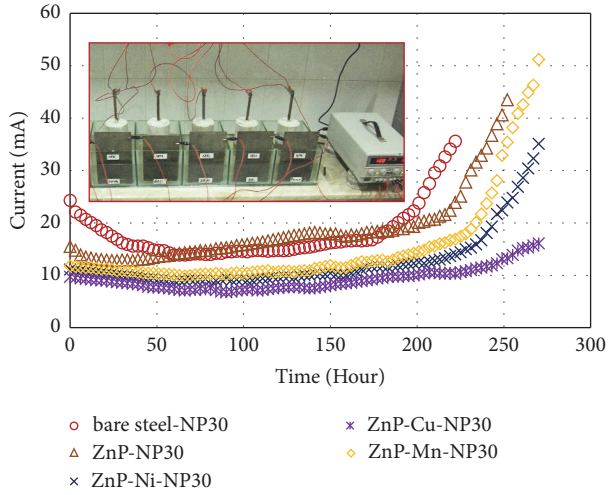

Figure 12: Time to cracking of RC specimens made with NP30-based cement and phosphated steel rebars after 28 days of curing.

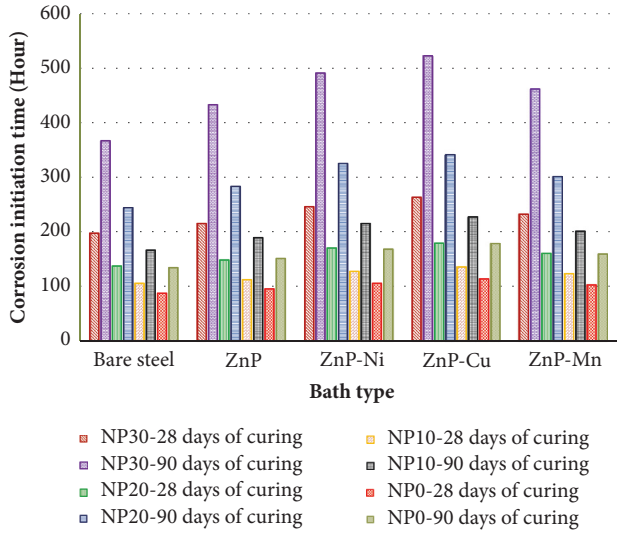

Figure 13: Average corrosion times of RC specimens at 28 and 90 days of curing (straight rebars).

corrosion resistance was noted in the following system: ZnP-Cu bath-NP30-based cement. The ZnP-Cu coated steel rebars embedded in NP30-based concrete have taken about 4 times longer duration for crack initiation than the bare steel rebars embedded in NP0-based concrete. The test lasted for 261 and 523 h in this specimen after 28 and 90 days of curing times, respectively.

This delay in corrosion time can be attributed to the following: (i) The pozzolanic reaction between glassy phase in NP and CH released during cement hydration contributes to filling the voids and pores in concrete with an additional C-S-H. This leads to decrease of pore size and to a smaller effective diffusivity for chloride [36]. This, which was confirmed by the water penetration depth, chloride penetrability, and concrete porosity tests, can also improve the long-term corrosion resistance of RC structures and make concrete denser and less permeable [36, 50]. (ii) The role of Cu^{2+} cation in refinement of the coating was confirmed by SEM and EDX analysis, Figure 7. (iii) The deposition of Cu^{2+}-based layer on the phosphated steel rebars contributes to forming a physical barrier between the base metal (steel) and its environment. (iv) Bication baths enhance the alkaline stability of the zinc phosphate coatings. According to Simescu and Idrissi [11] study, the dissolution of ZnP-Ni coating in the alkaline medium (pH ~12.5) is accompanied by the formation of hydroxyapatite $Ca_{10}(PO_4)_6(OH)_2$. Hydroxyapatite formation occurs even in the presence of aggressive chloride ions [11]. This chemical compound provides an effective protection against reinforcement corrosion and contributes to the reduction in chloride aggressiveness [10]. (v) Adding NP as cement replacement reduced pH values of concrete as seen in Table 4. This reduction can be due to the consumption of CH through the pozzolanic reaction and the lower cement content (i.e., the dilution effect).

From this accelerated test, it is also confirmed that the bication phosphating baths have higher corrosion resistance when compared to the monocation bath at all replacement levels of NP.

Further, it is worth mentioning that the bending action did not negatively affect the corrosion resistance of the phosphated steel rebars. The maximum reduction which was noted in ZnP treated rebar did not exceed 6%.

3.4. Bond Strengths. The bond stresses at 0.25 mm slip and at failure were presented in Table 5. It can be clearly seen that phosphate coatings applied to the embedded steel did not significantly reduce the bond strength of steel with concrete. After 28 days of curing, some of the phosphating baths increased the bond strength (i.e., ZnP-Cu, ZnP-Ni) while the other slightly decreased the bond strength with concrete (i.e., ZnP-Mn and ZnP). However, after 90 days of curing, all phosphated steel rebars achieved higher bond strengths when compared with the bare steel embedded in the control concrete.

3.5. Corrosion Behavior of Coated and Bare Steel in (CH-Cl) Solution. The open circuit potential values which were recorded after stabilization for the coated and bare steel specimens are illustrated in Figure 14. The results show that the potentials are becoming more noble for bication zinc phosphate coatings, and the ZnP-Cu coating is the most noble one. However, an inversion appears for the monocation zinc phosphate coating (i.e., ZnP bath). This, according to the author, can be explained by the following:

(i) The presence of Cu or Ni in the bication zinc phosphate coatings may increase the potential values, as copper and nickel are more noble than steel.

(ii) The formation of passive phases may make the potential more noble over time. This was confirmed by SEM, EDX, and XRD analysis, as shown in Figures 17–20.

(iii) The additives contribute to refinement of zinc phosphate crystals [26].

The polarization curves are shown in Figure 15. Upon increasing the potential above E_{corr} which corresponds to the minimum current density, a passive region was observed where the current density was of the order of $\mu A/cm^2$. Pitting

Table 5: Bond stresses (MPa) of the investigated phosphate steel rebars.

Concrete type	Rebar type	Bond stresses (MPa)			
		28 days of curing		90 days of curing	
		at 0.25 mm slip	at failure	at 0.25 mm slip	at failure
NP0	Bare steel	8.21	14.23	8.64	15.09
	ZnP	7.93	13.79	8.61	15.47
	ZnP-Ni	8.45	14.34	8.87	16.08
	ZnP-Cu	8.28	14.41	8.91	15.88
	ZnP-Mn	8.14	14.03	8.78	15.27
NP10	Bare steel	8.05	13.96	8.75	15.51
	ZnP	7.87	13.81	8.79	15.69
	ZnP-Ni	8.44	13.96	9.14	16.58
	ZnP-Cu	8.31	14.31	8.97	15.89
	ZnP-Mn	8.06	13.85	8.95	15.73
NP20	Bare steel	8.23	15.09	8.69	15.54
	ZnP	8.11	15.01	9.1	15.69
	ZnP-Ni	8.56	15.61	8.95	15.98
	ZnP-Cu	8.49	15.74	8.77	16.04
	ZnP-Mn	8.19	14.98	8.85	15.66
NP30	Bare steel	8.51	15.34	9.04	15.83
	ZnP	8.46	15.09	8.81	15.95
	ZnP-Ni	8.97	16.32	9.23	16.69
	ZnP-Cu	8.60	15.96	9.11	16.48
	ZnP-Mn	8.51	15.51	9.03	16.01

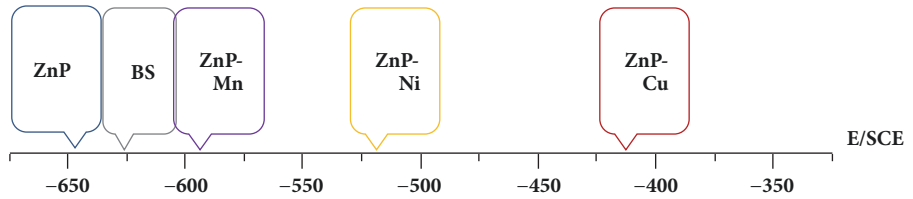

Figure 14: OCP values of the obtained coatings after stabilization.

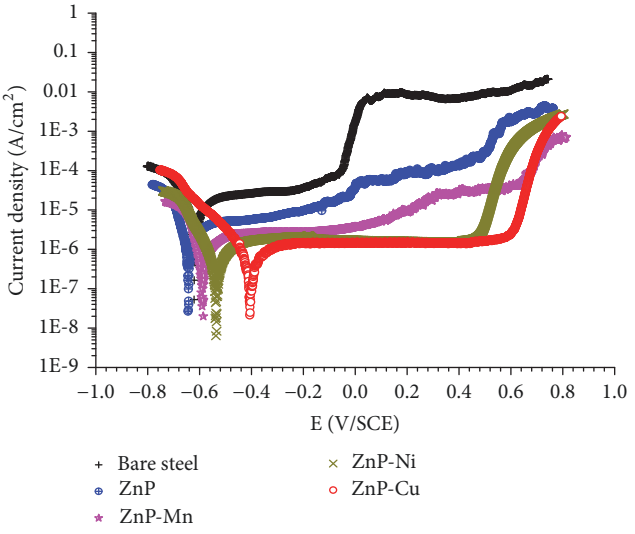

Figure 15: Polarization curves for zinc phosphate coating and bare steel after immersion in (CH-Cl) solution.

occurred in the bare steel at a potential value of less than zero. On the other hand, at potential values higher than 0.6 V/SCE an increase in the current density was observed in ZnP-Cu and ZnP-Ni specimens. This sharp increase in the current density corresponds to the pitting potential E_{pit}. Due to the effective barrier offered by the bication zinc phosphate coatings, the average polarization current declines considerably as compared to the bare steel. Table 6 presents E_{corr}, I_{corr}, E_{pit}, and passivity range of specimens after the polarization test. Among all the investigated coatings, the ZnP-Cu and ZnP-Ni coated specimens exhibited the lowest values of I_{corr}, about twentyfold lower with respect to the bare steel. In addition, these coatings revealed a passive region of about 1000 mV. The inhibition efficiency (IE) has further been estimated using the following equation [59]:

$$IE = \frac{[(I_{corr})_0 - I_{corr}]}{[(I_{corr})_0]} \quad (4)$$

Here $(I_{corr})_0$ and I_{corr} denote corrosion current density of reinforcing steel in the absence and presence of zinc

Table 6: I_{corr}, E_{corr}, E_{pit}, the passivity range, and the inhibition efficiency for the coated steel specimens and the bare steel.

Zinc phosphate bath	I (μA/cm^2)	E_{corr} (V/SCE)	E_{pit} (V/SCE)	Passivity range (V/SCE)	Inhibition efficiency (%)
Bare steel (Reference)	10.3	-0.626	-0.081	0.545	-
ZnP	2.4	-0.646	0.134	0.78	76.7
ZnP-Mn	1.6	-0.586	0.243	0.829	84.5
ZnP-Ni	0.7	-0.521	0.468	0.989	93.2
ZnP-Cu	0.5	-0.416	0.594	1.01	95.1

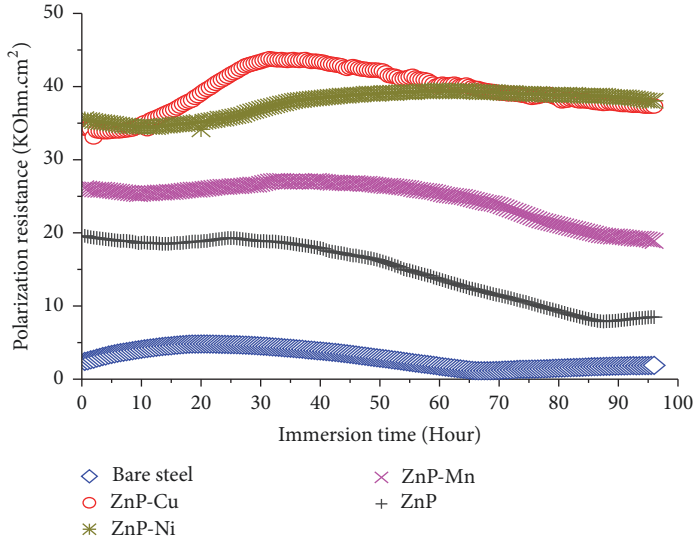

Figure 16: Polarization resistance over time of coated steel specimens and bare steel after 96 h of immersion in (CH-Cl) solution.

phosphate coating, respectively. As illustrated in Table 6, inhibition efficiency values of more than 90% were observed in the zinc phosphate coatings modified by either Cu^{2+} or Ni^{2+} cations. This result suggests that ZnP-Cu and ZnP-Ni coatings provide an effective corrosion resistance.

The periodic measurements of linear polarization resistance are displayed in Figure 16. For the bication zinc phosphate coatings, the differences in the behavior are not very significant. The polarization resistance decreases slightly at the beginning of the immersion, meaning that the dissolution rate of the bication coating slows down; then the polarization resistance increases, probably due to the formation of a passive phase by the resulting products. This result was confirmed by SEM, EDX, and XRD analysis, as shown in Figures 17–20. The formation of more than one passive phase, even in the presence of chloride ions can clearly be seen in Figure 19. These passive phases led to a better protection of steel as evidenced by the polarization tests; I = f(E) and R_p = f(t). After 96 h of immersion in the (CH-Cl) solution, ZnP-Cu and ZnP-Ni coatings recorded polarization resistance of about 40 kOhm.cm^2. On the other hand, the polarization resistance of the bare steel and the monocation coating recorded values of less than 10 kOhm.cm^2.

Based on the XRD analysis, the presence of calcium hydroxyzincate, $Ca(Zn(OH)_3)_2.2H_2O$, is clearly seen in all zinc phosphate coatings after 96 h of immersion in the (CH-Cl) solution. This compound is the main corrosion product of galvanised steel in chloride contaminated concrete [60, 61]. New peaks related to the formation of other products, such as hydroxyapatite, $Ca_{10}(PO_4)_6(OH)_2$, and copper oxide were detected in ZnP-Cu coating. The formation of such passive products in a highly alkaline solution contaminated with chloride ions was reported by other researchers [9–11, 62]. These products contribute to the decrease of the chloride aggressiveness and provide an effective protection against the reinforcement corrosion, although further investigation is needed to study their electrochemical behavior in a wider range of pH and at different chloride ion concentrations. It is worth mentioning that the copper particles deposited in the zinc phosphating remained intact as evidenced by the strong peaks of copper shown in either EDX analysis or XRD diffraction test. Compared with that of bication baths, the monocation bath has the worst corrosion performance where uncovered steel zones can easily be distinguished in Figure 17. These zones are attributed to the rapid dissolution of the phosphating coating and the complete breakdown of the local passive layer.

4. Conclusions

This paper was an attempt to investigate the effects of some additives such as alkali metal ions on zinc phosphate bath properties. In addition, the effect of using NP-based binders on corrosion performance was mainly studied.

(i) Bication baths led to improvements in the zinc phosphate coating performance in terms of reinforcement

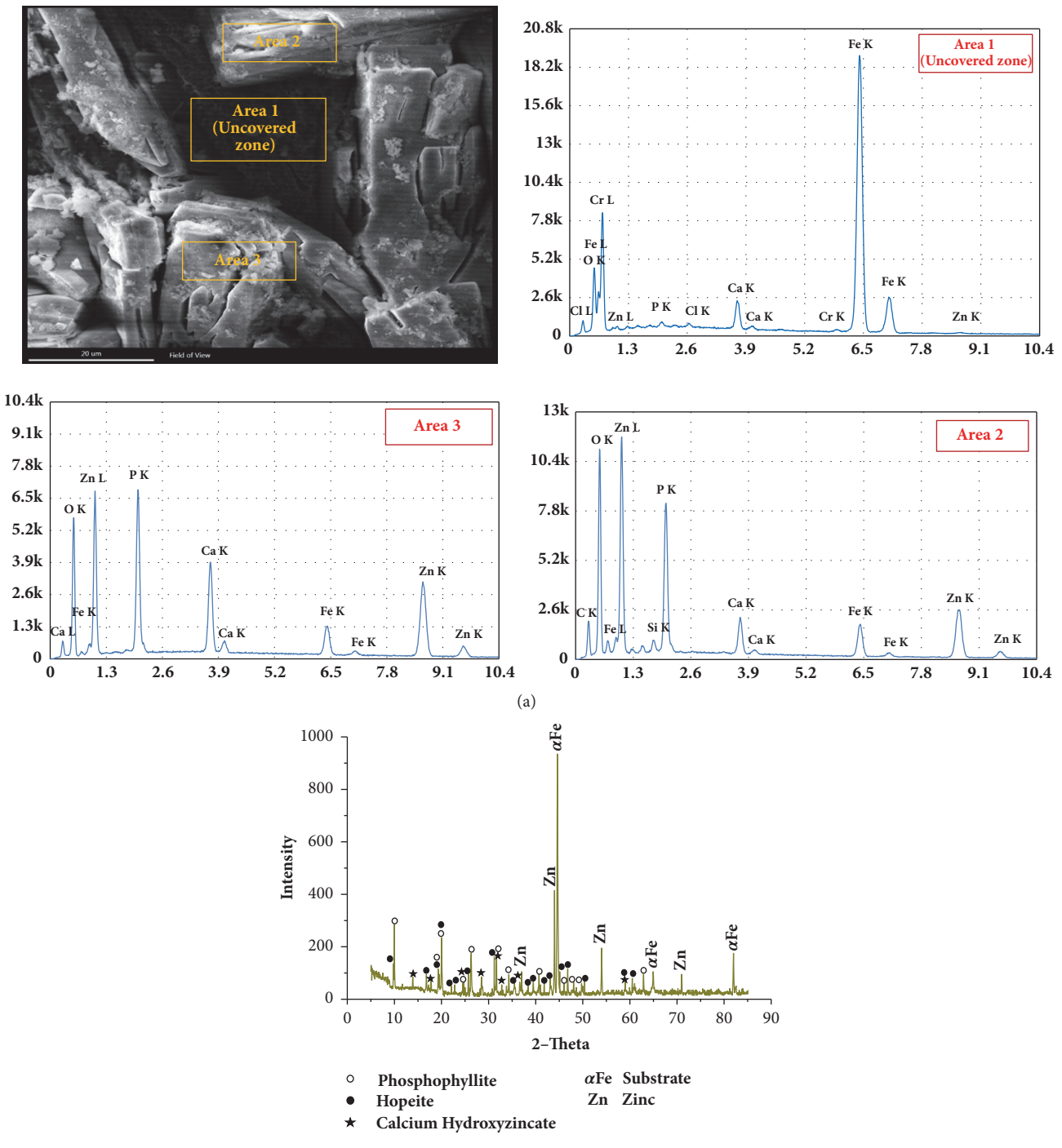

Figure 17: SEMs and EDX (a) and XRD analysis (b) of ZnP coating after immersion in (CH-Cl) solution for 96 h.

corrosion resistance and bond strength between concrete and steel. The best corrosion resistance was observed in the ZnP-Cu-NP30-based binder system. It took corrosion initiation periods 4 times longer than the bare steel-NP0-based cement system. The reduced chloride penetrability, water permeability, and porosity of NP-based concrete specimens made a further significant improvement in terms of reinforcement corrosion resistance. A similar excellent corrosion performance was also noted in the ZnP-Ni system, as it performed very well in the electrochemical tests carried out using either (CH-Cl) solution or concrete specimens. Although ZnP-Mn coating performed, to some extent, well, but its corrosion performance was not as high as the ZnP-Cu and ZnP-Ni coatings.

(ii) Bent phosphated steel rebars did not significantly affect the corrosion performance.

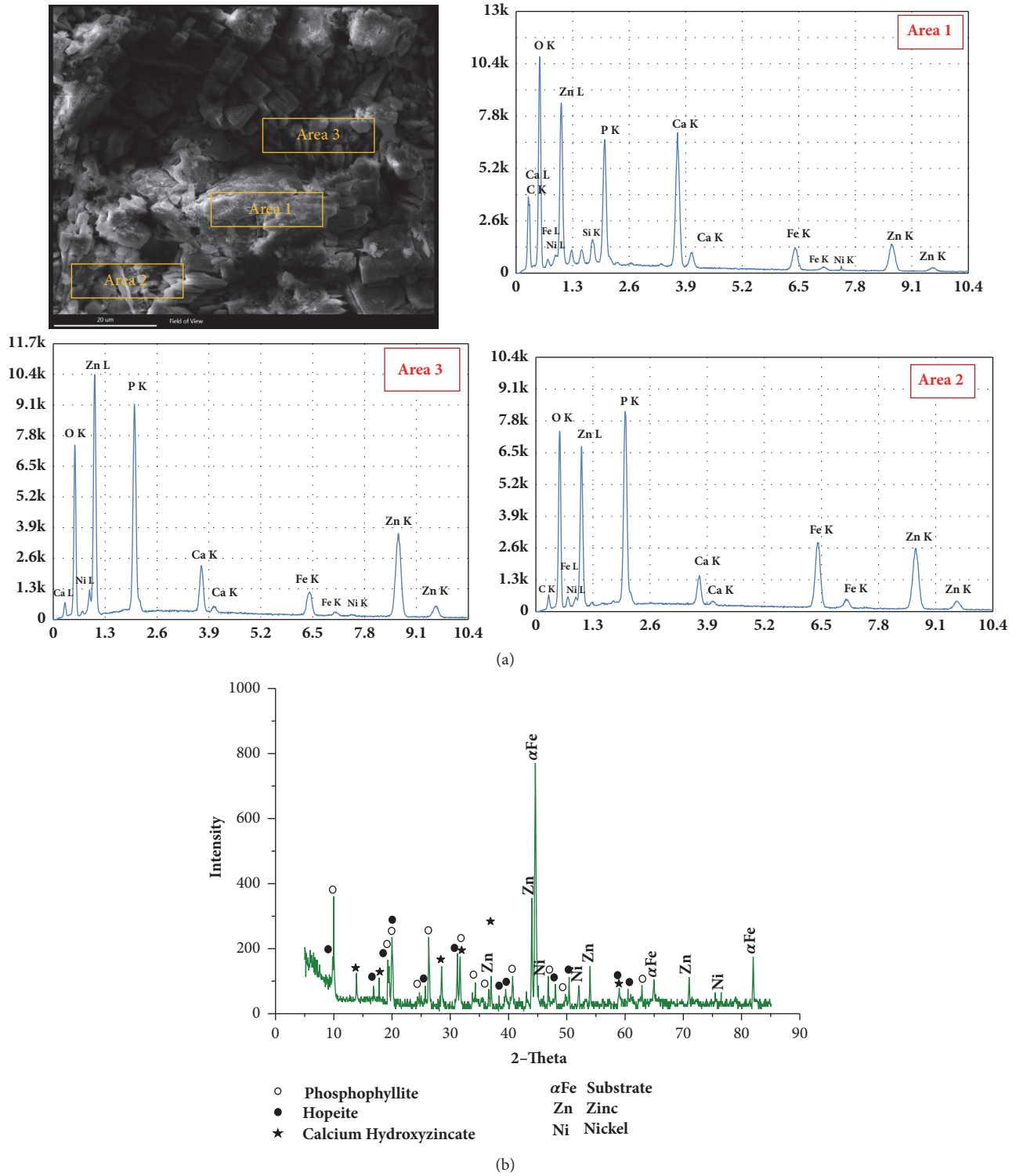

Figure 18: SEMs and EDX (a) and XRD analysis (b) of ZnP-Ni coating after immersion in (CH-Cl) solution for 96 h.

(iii) Based on the results of bond strength, it should be noted that the hydrogen embrittlement which can be encountered in acidic baths may be considered negligible in the studied phosphating baths.

(iv) The stability of the phosphate layer in a highly alkaline solution was significantly increased by modifying the zinc phosphating bath with Cu^{2+}, Ni^{2+}, and Mn^{2+}.

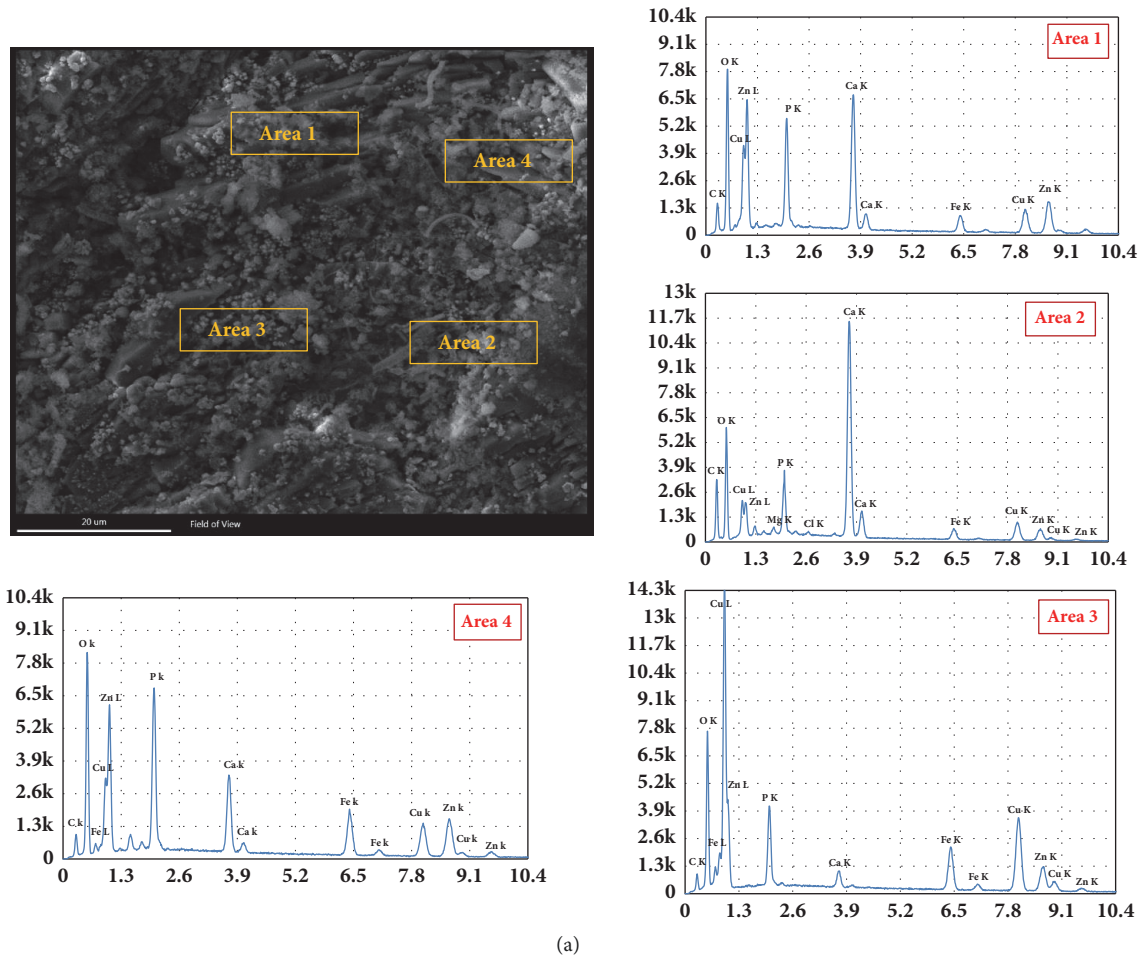

(a)

(b)

Figure 19: SEMs and EDX (a) and XRD analysis (b) of ZnP-Cu coating after immersion in (CH-Cl) solution for 96 h.

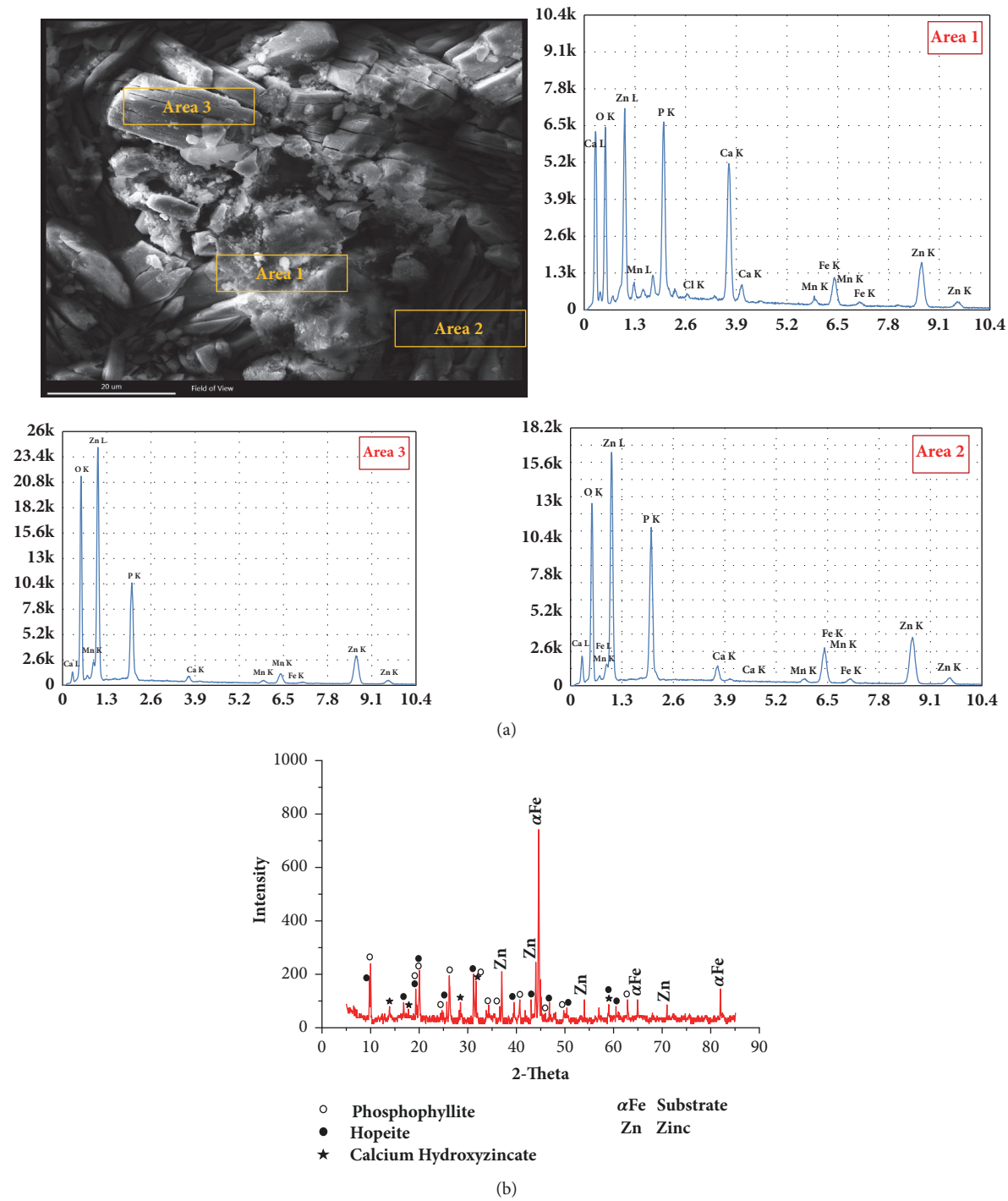

Figure 20: SEMs and EDX (a) and XRD analysis (b) of ZnP-Mn coating after immersion in (CH-Cl) solution for 96 h.

(v) Electrochemical test results revealed that the bication coatings performed very well in highly alkaline solutions contaminated with chloride ions. The inhibition efficiency values ranged from about 85% to 95%. The SEM, EDX, and XRD analysis supported this result, where passive resulting products were detected.

(vi) The microscopical examination of the monocation bath specimens, after the polarization resistance test, revealed uncovered steel zones, indicating that corrosion performance of this bath may not be relied upon.

(vii) Further studies on the chemical stability of the modified zinc phosphate coatings are highly recommended. Long-term tests when these coatings are exposed to chloride ions are also recommended. Testing the efficiency of the formed phosphate coatings when immersed in concrete exposed to carbonation is recommended, as well.

(viii) Finally, there is a need to develop an optimum chemical composition of the phosphating bath and treatment conditions that provide maximum protection against reinforcement corrosion.

Data Availability

The data used to support the findings of this study are available from the corresponding author upon request.

Conflicts of Interest

The author declares that there are no conflicts of interest regarding the publication of this paper.

References

[1] A. Neville, "Chloride attack of reinforced concrete: an overview," *Materials and Structures*, vol. 28, no. 2, pp. 63–70, 1995.

[2] G. J. Verbeck, "Mechanisms of Corrosion of Steel in Concrete," in *Corrosion of Metals in Concrete*, vol. SP-49, pp. 21–38, American Concrete Institute, 1975.

[3] A. Poursaee, "Corrosion protection methods of steel in concrete," *Corrosion of Steel in Concrete Structures*, pp. 241–248, 2016.

[4] L. Bertolini, B. Elsener, P. Pedeferri, E. Redaelli, and R. Polder, *Corrosion of Steel in Concrete: Prevention, Diagnosis, Repair*, vol. 12, 69469, Wiley-VCH Verlag GmbH Co. Boschstr, Weinheim, Germany, 2nd edition, 2003.

[5] B. Elsener, *Corrosion Inhibitors for steel in concrete-state of the art report*, vol. 35, EFC publication. IOM Communications, London, 2001.

[6] J. Carmona, P. Garcés, and M. A. Climent, "Efficiency of a conductive cement-based anodic system for the application of cathodic protection, cathodic prevention and electrochemical chloride extraction to control corrosion in reinforced concrete structures," *Corrosion Science*, vol. 96, pp. 102–111, 2015.

[7] C. M. Hansson, "Corrosion of stainless steel in concrete," in *Corrosion of Steel in Concrete Structures*, A. Poursaee, Ed., Elsevier Ltd., 2016.

[8] M. Ormellese, F. Bolzoni, S. Goidanich, M. P. Pedeferri, and A. Brenna, "Corrosion inhibitors in reinforced concrete structures Part 3 - Migration of inhibitors into concrete," *Corrosion Engineering, Science and Technology*, vol. 46, no. 4, pp. 334–339, 2011.

[9] A. A. Elshami, S. Bonnet, A. Khelidj, and L. Sail, "Novel anticorrosive zinc phosphate coating for corrosion prevention of reinforced concrete," *European Journal of Environmental and Civil Engineering*, vol. 21, no. 5, pp. 572–593, 2017.

[10] F. Simescu and H. Idrissi, "Effect of zinc phosphate chemical conversion coating on corrosion behaviour of mild steel in alkaline medium: protection of rebars in reinforced concrete," *Science and Technology of Advanced Materials*, vol. 9, no. 4, p. 045009, 2008.

[11] F. Simescu and H. Idrissi, "Corrosion behaviour in alkaline medium of zinc phosphate coated steel obtained by cathodic electrochemical treatment," *Corrosion Science*, vol. 51, no. 4, pp. 833–840, 2009.

[12] O. Girciene, R. Ramanauskas, L. Gudaviciute, and A. Martuiene, "Formation of conversion ZnNiMn phosphate coatings on steel and corrosion behaviour of phosphated specimens in a chloride-contaminated alkaline solution," *Chemiji*, vol. 24, pp. 182–189, 2013.

[13] P. Zarras. and J. D. Stenger-Smith, "Smart Inorganic and Organic Pretreatment Coatings for the Inhibition of Corrosion on Metals/Alloys," in *Intelligent Coatings for Corrosion Control*, A. Tiwari and etal., Eds., Butterworth-Heinemann, 2015.

[14] D. G. Weldon, *Failure Analysis of Paints and Coatings*, John Wiley & Sons, Ltd, 2009.

[15] M. Tamilselvi, P. Kamaraj, M. Arthanareeswari, S. Devikala, and J. A. Selvi, "Development of nano SiO2 incorporated nano zinc phosphate coatings on mild steel," *Applied Surface Science*, vol. 332, pp. 12–21, 2015.

[16] F. Fang, J.-H. Jiang, S.-Y. Tan, A.-B. Ma, and J.-Q. Jiang, "Characteristics of a fast low-temperature zinc phosphating coating accelerated by an ECO-friendly hydroxylamine sulfate," *Surface and Coatings Technology*, vol. 204, no. 15, pp. 2381–2385, 2010.

[17] D. R. Harris and P. Casey, "Formulating Surface Coatings," in *Active Protective Coatings*, vol. 233 of *Springer Series in Materials Science*, pp. 85–104, Springer Netherlands, Dordrecht, 2016.

[18] D. Grigoriev, "Anticorrosion Coatings with Self Recovering Ability Based on DamageTriggered Micro- and Nanocontainers," in *Intelligent Coatings for Corrosion Control*, A. Tiwari and etal., Eds., Butterworth-Heinemann, 2015.

[19] O. Girčiene, R. Ramanauskas, V. Burokas, and A. Martušiene, "Formation of phosphate coatings on steel and corrosion performance of phosphated specimens in alkaline solutions," *Transactions of the IMF*, vol. 82, no. 5-6, pp. 137–140, 2004.

[20] R. Zeng, Z. Lan, L. Kong, Y. Huang, and H. Cui, "Characterization of calcium-modified zinc phosphate conversion coatings and their influences on corrosion resistance of AZ31 alloy," *Surface and Coatings Technology*, vol. 205, no. 11, pp. 3347–3355, 2011.

[21] N. Rezaee, M. M. Attar, and B. Ramezanzadeh, "Studying corrosion performance, microstructure and adhesion properties of a room temperature zinc phosphate conversion coating containing Mn2+ on mild steel," *Surface and Coatings Technology*, vol. 236, pp. 361–367, 2013.

[22] M. M. Jalili, S. Moradian, and D. Hosseinpour, "The use of inorganic conversion coatings to enhance the corrosion resistance of reinforcement and the bond strength at the rebar/concrete," *Construction and Building Materials*, vol. 23, no. 1, pp. 233–238, 2009.

[23] D. Zimmermann, A. G. Muñoz, and J. W. Schultze, "Microscopic local elements in the phosphating process," *Electrochimica Acta*, vol. 48, no. 20-22, pp. 3267–3277, 2003.

[24] M. Manna, A. Shah, and S. V. Kulkarni, " Development of phosphate coating on the surface of TMT rebar: an option to study the effect of n-SiO ," *Ironmaking & Steelmaking*, vol. 44, no. 9, pp. 666–675, 2016.

[25] M. Sheng, Y. Wang, Q. Zhong, H. Wu, Q. Zhou, and H. Lin, "The effects of nano-SiO2 additive on the zinc phosphating of carbon steel," *Surface and Coatings Technology*, vol. 205, no. 11, pp. 3455–3460, 2011.

[26] A. A. al-Swaidani, "Modified Zinc Phosphate Coatings: A Promising Approach to Enhance the Anti-Corrosion Properties of Reinforcing Steel," *MOJ Civil Engineering*, vol. 3, no. 5, 2017.

[27] D. B. Freeman, *Phosphating and Metal Pre-Treatment*, Woodhead-Faulkner, Cambridge, UK, 1986.

[28] S. K. Rahimi, R. Potrekar, N. K. Dutta, and N. R. Choudhury, "Anticorrosive interfacial coatings for metallic substrates," *Surface Innovations*, vol. 1, no. 2, pp. 112–137, 2013.

[29] J. Donofrio, "Zinc phosphating," *Metal Finishing*, vol. 108, no. 11-12, pp. 40–56, 2010.

[30] H. Kunst et al., *Metals, Surface Treatment, Encyclopedia of industrial chemistry*, Wiley-VCH Verlag GmbH & Co. KGaA, Weinheim, 2012.

[31] D. Weng, P. Jokiel, A. Uebleis, and H. Boehni, "Corrosion and protection characteristics of zinc and manganese phosphate coatings," *Surface and Coatings Technology*, vol. 88, no. 1-3, pp. 147–156, 1997.

[32] K. Ogle, A. Tomandl, N. Meddahi, and M. Wolpers, "The alkaline stability of phosphate coatings I: ICP atomic emission spectroelectrochemistry," *Corrosion Science*, vol. 46, no. 4, pp. 979–995, 2004.

[33] A. Tomandl, M. Wolpers, and K. Ogle, "The alkaline stability of phosphate coatings II: In situ Raman spectroscopy," *Corrosion Science*, vol. 46, no. 4, pp. 997–1011, 2004.

[34] M. Shoeib, M. Farouk, and F. Hanna, "Influence of ethoxylate surfactants on zinc phosphate coatings," *Metal Finishing*, vol. 95, no. 9, pp. 62–68, 1997.

[35] K. Ogle and R. G. Buchheit, *Conversion Coatings, Corrosion Protection. Encyclopedia in electrochemistry*, 2007.

[36] A. M. al-Swaidani and S. D. Aliyan, "Effect of adding scoria as cement replacement on durability-related properties," *International Journal of Concrete Structures and Materials*, vol. 9, no. 2, pp. 241–254, 2015.

[37] N. Kouloumbi, G. Batis, and P. Pantazopoulou, "Efficiency of natural Greek pozzolan in chloride-induced corrosion of steel reinforcement," *Cement, Concrete and Aggregates*, vol. 17, no. 1, pp. 18–25, 1995.

[38] M. I. Khan and A. M. Alhozaimy, "Properties of natural pozzolan and its potential utilization in environmental friendly concrete," *Canadian Journal of Civil Engineering*, vol. 38, no. 1, pp. 71–78, 2010.

[39] M. R. Moufti, A. A. Sabtan, O. R. El-Mahdy, and W. M. Shehata, "Assessment of the industrial utilization of scoria materials in central Harrat Rahat, Saudi Arabia," *Engineering Geology*, vol. 57, no. 3-4, pp. 155–162, 2000.

[40] G. K. Al-Chaar, M. Alkadi, and P. G. Asteris, "Natural pozzolan as a partial substitute for cement in concrete," *The Open Construction & Building Technology Journal*, vol. 7, pp. 33–42, 2013.

[41] Y. Senhadji, G. Escadeillas, H. Khelafi, M. Mouli, and A. S. Benosman, "Evaluation of natural pozzolan for use as supplementary cementitious material," *European Journal of Environmental and Civil Engineering*, vol. 16, no. 1, pp. 77–96, 2012.

[42] V. Saraswathy, S. Muralidharan, K. Thangavel, and S. Srinivasan, "Influence of activated fly ash on corrosion-resistance and strength of concrete," *Cement and Concrete Composites*, vol. 25, no. 7, pp. 673–680, 2003.

[43] GEMGR "the General Establishment of Geology and Mineral Resources" in Syria (2017). Official document no. (3207/T/9), dated 21.11.2007 (in Arabic).

[44] A. Al-Swaidani, A. Soud, and A. Hammami, "Improvement of the Early-Age Compressive Strength, Water Permeability, and Sulfuric Acid Resistance of Scoria-Based Mortars/Concrete Using Limestone Filler," *Advances in Materials Science and Engineering*, vol. 2017, pp. 1–17, 2017.

[45] A. M. Neville, *Properties of concrete*, Pearson Education, Fifth, 2011.

[46] V. Horsakulthai, S. Phiuvanna, and W. Kaenbud, "Investigation on the corrosion resistance of bagasse-rice husk-wood ash blended cement concrete by impressed voltage," *Construction and Building Materials*, vol. 25, no. 1, pp. 54–60, 2011.

[47] A. K. Parande, B. Ramesh Babu, M. Aswin Karthik, K. K. Deepak Kumaar, and N. Palaniswamy, "Study on strength and corrosion performance for steel embedded in metakaolin blended concrete/mortar," *Construction and Building Materials*, vol. 22, no. 3, pp. 127–134, 2008.

[48] T. Ha, S. Muralidharan, J. Bae et al., "Accelerated short-term techniques to evaluate the corrosion performance of steel in fly ash blended concrete," *Building and Environment*, vol. 42, pp. 78–85, 2007.

[49] V. Saraswathy and H.-W. Song, "Corrosion performance of rice husk ash blended concrete," *Construction and Building Materials*, vol. 21, no. 8, pp. 1779–1784, 2007.

[50] E. Guneyisi, T. Ozturan, and M. Gesoglu, "A study on reinforcement corrosion and related properties of plain and blended cement concretes under different curing conditions," *Cement Concrete Composites*, vol. 27, pp. 449–461, 2005.

[51] G. Xing, C. Zhou, T. Wu, and B. Liu, "Experimental study on bond behavior between plain reinforcing bars and concrete," *Advances in Materials Science and Engineering*, Article ID 604280, 2015.

[52] A. Poursaee, "Corrosion of steel bars in saturated Ca(OH)2 and concrete pore solution," *Concrete Research Letters*, vol. 1, no. 3, p. 90, 2010.

[53] Z. Panossian, "Phosphating of Steel for Cold Forming Processes," in *Encyclopedia of Tribology*, Q. J. Wang and Y. W. Chung, Eds., Springer, 2013.

[54] A. V. Sandu, C. Coddet, and C. Bejinariu, "Study on the chemical deposition on steel of zinc phosphate with other metallic cations and hexamethilen tetramine: I. Preparation and structural and chemical characterization," *Chemistry Magazine*, vol. 63, no. 4, pp. 401–406, 2012.

[55] H.-Y. Su and C.-S. Lin, "Effect of additives on the properties of phosphate conversion coating on electrogalvanized steel sheet," *Corrosion Science*, vol. 83, pp. 137–146, 2014.

[56] S. A. Kulinich and A. S. Akhtar, "On conversion coating treatments to replace chromating for Al alloys: Recent developments and possible future directions," *Russian Journal of Non-Ferrous Metals*, vol. 53, no. 2, pp. 176–203, 2012.

[57] K. Abdalla, A. Rahmat, and A. Azizan, "Effect of copper (II) acetate pretreatment on zinc phosphate coating morphology and corrosion resistance," *Journal of Coatings Technology and Research (JCTR)*, vol. 10, no. 1, pp. 133–139, 2013.

[58] A. M. Al-Swaidani, "Production of more durable and sustainable concretes using volcanic scoria as cement replacement," *Materiales de Construcción*, vol. 67, no. 326, 2017.

[59] B. Assouli, A. Srhiri, and H. Idrissi, "Effect of 2-mercaptobenzimidazole and its polymeric film on the corrosion inhibition of brass (60/40) in ammonia solution," *Corrosion*, vol. 60, no. 4, pp. 399–407, 2004.

[60] F. Belaid, G. Arliguie, and R. Francois, "Corrosion products of galvanized rebars embedded in chloride-contaminated concrete," *Corrosion*, vol. 56, no. 9, pp. 960–965, 2000.

[61] M. A. Arenas, C. Casado, V. Nobel-Pujol, and J. De Damborenea, "Influence of the conversion coating on the corrosion of galvanized reinforcing steel," *Cement and Concrete Composites*, vol. 28, no. 3, pp. 267–275, 2006.

[62] L. E. A. Berlouis, D. A. Mamman, and I. G. Azpuru, "The electrochemical behaviour of copper in alkaline solutions containing fluoride, studied by in situ ellipsometry," *Surface Science*, vol. 408, no. 1-3, pp. 173–181, 1998.